Effect of primary driers on oxidative drying of high-solid alkyd binder: Investigation of thickness effects by mechanical tests and infrared spectroscopy.

Iva Charamzová,[a] Jaromír Vinklárek,[b] and Jan Honzíček [a,*]

[a] Institute of Chemistry and Technology of Macromolecular Materials, Faculty of Chemical Technology, University of Pardubice, Studentská 573, 532 10 Pardubice, Czech Republic.

[b] Department of General and Inorganic Chemistry, Faculty of Chemical Technology, University of Pardubice, Studentská 573, 532 10 Pardubice, Czech Republic.

[*] Corresponding author. Tel: +420/46603 7229. Fax: +420/46603 7068

E-mail address: jan.honzicek@upce.cz (J. Honzíček)

Keywords: alkyd resin; autoxidation; infrared spectroscopy

Highlights:

Detailed study of oxidative drying on high-solid alkyd coatings.

Effect of various metal-based driers was established.

Thickness effect was determined by ATR-infrared spectroscopy.

Graphical Abstract:

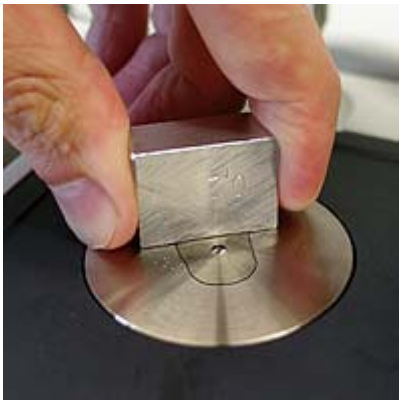

Abstract:

Catalytic activity of four primary driers was investigated in high-solid alkyd binder modified with tall oil fatty acids. The drying activity was established by mechanical tests. Infrared spectroscopy was used for detailed investigation of chemical changes during the autoxidation process. Due to strong thickness effect, the infrared

study was performed using attenuated total reflectance (ATR) technique, which measures spectra of a thin layer from the interface sample/ATR crystal (down surface of the sample). Coatings of 30 μm-wet thickness were found to be enough thin to be considered as a homogenously dried bulk with negligible effect of oxygen diffusion. It makes the 30 μm-layers very suitable for determination of kinetic parameters of the autoxidation process. For the first time, ATR-IR experiments on several samples of the same composition but different film thickness were used for detailed investigation of the thickness effect.

Two well-distinguished modes of film-formation were observed in studied drier/binder systems. Front front-forming drying occurs when the autoxidation is fast and air-oxygen diffusion is slower than its consumption. In extreme case, the film-formation process is practically ceased because impermeable skin is formed and the coating is not through-dried for very long time. The second mode, homogenous drying, is observed when autoxidation is slow and oxygen consumption is not fast enough to establish oxygen gradient in the coating.

1. Introduction

Saturated polyester resins modified with vegetable oils, known as alkyd resins, have been established as significant group of air-drying paint binders used in protective and decorative coatings [1]. In last few decades, the formulations based on alkyd resins have reached great attention mainly due to high content of material available from renewable sources [2, 3]. Modern alkyd paints suitable for industry and hobby market are based on high-solid (HS) and water-borne (WB) formulation fulfilling ecological concerns about low emission of volatile organic compounds (VOC) [4]. The HS formulations, with less than 30 % of solvents, usually contain polymers of low molecular weight, high functionality and special architecture that ensures low viscosity and satisfactory film-forming properties [5]. In case of alkyd resins, it is usually not necessary to build particles with core-shell structure as the requirements are provided by hard polyester backbone covered by soft polyunsaturated fatty acid chains (Scheme 1). After solvent evaporation, the HS alkyd layer stays liquid. Both sol-gel transition and hardening process are based solely on the cross-linking of the fatty acid tails, which occurs in the presence of air-oxygen. Such process, known as autoxidation, is generally very slow at ambient temperature and has to be catalyzed by transition metal compounds, so-called driers [6, 7]. These catalysts considerably reduce drying time and improve physical properties of final polymeric film. In case of HS formulation, the role of drier is crucial for film-forming process owing to negligible contribution from physical drying. Cobalt carboxylates (*e.g.* cobalt(II) 2-ethylhexanoate, **Co**) are powerful alkyd driers well established in paint producing industry. Nevertheless, global demand for their replacement is constantly increasing due to ecological reasons [8, 9]. Various driers

based on vanadium [10-13], manganese [14-16] and iron [17-21], reported in literature, exhibit promising properties in alkyd formulation or liquid model systems (*e.g.* methyl linoleate). Unfortunately, recent comparative studies have revealed that cobalt compounds cannot be easily replaced. The alternatives show some differences in kinetics of the autoxidation process that leads to cured films of different properties [22, 23].

Various experimental methods, including liquid chromatography [24], mass spectrometry [25], measurements of oxygen uptake [26], measurements of viscoelastic properties on quartz crystal microbalance [27] and vibration spectroscopy [28, 29], have been used for investigation of the air-drying process on alkyd resins or their liquid model systems (*e.g.* fatty acids esters). Nevertheless, majority of these methods are suitable only for investigations of reaction mechanisms or determination of the reaction kinetics in homogenous mixtures saturated with air-oxygen. So far, only confocal Raman microscopy [16, 30] and NMR imaging [31, 32] were successfully used for description of thickness effect caused by concentration gradient of molecular oxygen.

The aim of this study is to establish time-resolved infrared spectroscopy (IR) as a method suitable for investigation of the thickness effect occurring upon the air-drying process. For this purpose, HS alkyd resin with high double bond density (CHS-ALKYD TI 870, **TI870**) was chosen, for which a strong effect of the film thickness is expected. The binder was cured with common cobalt-based drier **Co**, which performance is compared with three commercial alternatives; namely manganese 2-ethylhexanoate (**Mn**), vanadium compound VP 0132 (**V**) and iron bispidine complex (**Fe**). Before the detailed infrared study, behavior of each drier/binder combination was established by standard mechanical tests commonly used for paint testing. We note that each drier/binder system under study have shown a very different performance, which will be documented by mechanical tests and IR studies.

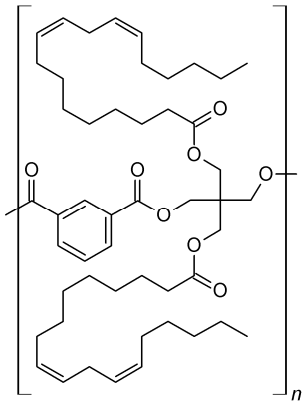

Scheme 1. Simplified structure of pentaerythritol-based HS alkyd resin. Tails of linoleic acid are shown as a representative of fatty acids suitable for oxidative drying.

2. Experimental section

2.1 Materials

Solventless alkyd resin based on tall oil fatty acids CHS-ALKYD TI 870 (**TI870**; oil length = 87 %, acid value = 8 mg KOH/g) was supplied by Spolchemie. The commercial drier cobalt(II) 2-ethylhexanoate (65 wt.% in mineral spirits; **Co**) was supplied by Sigma-Aldrich. Borchers VP0132 (**V**), Octa-Soligen Manganese 10 (manganese 2-ethylhexanoate; **Mn**), Borchi OXY-Coat (iron bispidine complex, 1 wt.% in 1,2-propylene glycol; **Fe**) were supplied by Borchers. Dearomatized white spirit (Thinner S 6006 Aromafree) was supplied by Severochema. All reported metal concentrations are given in wt.% based on solid of the alkyd resin.

2.2 Preparation of test coatings

Appropriate drier was treated with toluene (100 µl). Immediately after dissolution, it was treated with **TI870** (5.00 g) and vigorously stirred for 2 min to get a homogenous mixture. Viscosity of the formulation was reduced by dearomatized white spirit to 90 wt.% of solid content. Mixture was vigorously stirred for 2 min again and degassed in ultrasound bath (3 min in degas mode). The test films were casted on the substrate by frame applicators.

2.3 Film drying time

The drying performance has been determined by BK (Beck Koller) method on a Drying Time Recorder (BYK) according to ASTM D5895-03 [33] and under standard laboratory conditions (T = 23 °C, rel. humidity = 50 %). The instrument is a straight-line recorder equipped with hemispherical-ended needle (D = 1 mm). The films were casted on clean glass strips (305 × 25 × 2 mm) using frame applicators of 38 and 76 µm gaps. The needle was placed in horizontal direction at the beginning of the wet film and equipped with 5 g weight. The mark, appeared during 24 h, was used for the estimation four drying stages of given formulation. “Set-to-touch” time (τ_1) is reached when film stops flowing behind needle and pear-shape deformed film appears. During the second period needle gives bold and uninterrupted line revealing the glass substrate. It finishes, when the film is “tack-free” dry (τ_2). After this time, the needle starts to climb over the film. The needle tears the layer and lefts grove with wrinkled and distorted edges until the film is “dry-through” (τ_3). After τ_3, only very thin mark could be observed on the film [33].

2.4 Determination of film hardness

Film hardness development was monitored using a Pendulum Hardness Tester (Elcometer) with Persoz type pendulum in conformity with ISO 1522 [34] under standard laboratory conditions (T = 23 °C, rel. humidity = 50 %). The method is based on registering the number of pendulum swings it takes before the amplitude of the pendulum is damped to a certain extent. Test films were casted on glass plates (100 × 200 × 4 mm) using frame applicator of 90-μm gap and their properties were measured within 100 days (average value from three measurements is given). The obtained values were related to the hardness of a glass standard (limit value of the pendulum test) and expressed as relative hardness [35]. The error in determination of surface hardness was estimated to be 0.5 %.

2.5 Visual control and adhesion tests

Test formulations were cast on glass plates (100 × 200 × 4 mm) using frame applicators of 90 and 150 μm gaps and left horizontally for 72 hours to prevent certain surface defects such as paint spillage (runs) or changes in film thickness. After that the panels were stored for 100 days in vertical position under standard laboratory conditions (T = 23 °C, rel. humidity = 50 %). Appearance of cured films and visual defects were evaluated after 10 and 100 days of curing. The adhesion test was performed on the same coatings using a cross-cut tester (Zehntner) according to ISO 2409 [36]. Briefly, the tester was held vertically to test panel surface placed on a firm base. Lattice pattern was made by two successive cuts penetrating the coating down to substrate in 90° angle to each other. 75-mm long tape was centered over the grid and smoothly placed. The tape was removed 5 min. after applying, steadily in 0.5–1.0 s at an angle as close as possible to 60°. Resulting grid was evaluated according to percentage of removed area as follows: 0 (0 %), 1 (< 5 %), 2 (5–15 %), 3 (15–35 %), 4 (> 65 %), 5 (any degree of flaking that cannot be classified by classification 4).

2.6 Time-resolved infrared spectroscopy

The infrared spectra of alkyd coatings were measured on a FTIR spectrometer Nicolet iS50 in the range of 4000–500 cm^{-1} with the data spacing of 0.5 cm^{-1} (64 scans per spectrum) under standard laboratory conditions (T = 23 °C, rel. humidity = 50 %). Infrared spectra obtained by attenuated total reflectance (ATR) technique (built-in all-reflective diamond crystal) were registered every 5 min for 20 h. Formulations were casted by frame applicator on plate, where the sample has intimate contact to the ATR crystal. As the top surface of ATR crystal lays 20 μm above the sampling plate, the wet coating on the crystal was always 20 μm thicker than the gap of the frame applicator used. Collected series of the spectra were integrated in area 3025–2990 cm^{-1} using fixed two-

point baseline at 3025 and 2990 cm^{-1} [ν_a(*cis*-C=C–H)]. Rate coefficients ($-k_{CH,max}$) were obtained from logarithmic plots of integrated area *vs.* time as the steepest slope. The error in determination of ($-k_{CH,max}$) was less than 10 % (three independent measurements for each run). Induction time (IT) was estimated from the logarithmic plots graphically as intersection of horizontal line at 4.605 and tangential line extending the curve after knee point. Half-life of autoxidation process ($t_{1/2}$) was obtained from the integral plot, when the when the curve decreases to 50 % of initial intensity. The intensity of band at 989 cm^{-1} [γ(*cis-trans*-C=*C–H*)] was determined as the height of the band at this wavenumber using two-point baseline fixed at 998 and 957 cm^{-1}. Maximum on this curve was defined by time t_{conj}. The intensity of ν(O–H) was determined by integration in area 3550–3200 cm^{-1} using fixed two-point baseline at 3985 and 3120 cm^{-1}.

3. Results and discussion

*3.1 Drying performance of **Co**, **Mn**, **V** and **Fe***

Drying activity of four primary driers was evaluated in HS binder modified with tall oil fatty acids **TI870**. The samples of appropriate metal concentration were diluted with dearomatized white spirit to adjust viscosity of the formulation. The use of other additives (*e.g.* secondary driers and antiskinning agents) was avoided in order to estimate solely the effect of given primary driers. The film drying times (τ_1, τ_2 and τ_3; for definition see Section 2.3) of the alkyd formulations were estimated on coatings of 76 μm-wet thickness. The measurements on thinner coatings (38 μm-wet thickness) were performed in order to avoid entering in a regime where oxygen transport is the limiting factor. Development of relative hardness in time was measured on coatings of 90 μm-wet thickness resulting in ~35 μm dry film that is common in paint application. The thicker coatings were prepared for detection the tendency to form a surface with visual defects. We note that all systems under study have excellent adhesion to the glass substrate (degree 0 according to ISO 2409 [36]).

The activity of cobalt 2-ethylhexanoate (**Co**) was studied at concentrations 0.01–0.06 wt.% of the metal on solid content. Set-to-touch time (τ_1) rises with lowering of metal concentration but it is not influenced by film thickness (Table 1). Such observations imply fast solvent evaporation and almost homogenous cross-linking at the beginning of the autoxidation process. It is due to saturation of the formulation by air-oxygen before spreading sample over glass panel used for tests. Strong dependence on film thickness was observed only in the next phases of the oxidative drying. The tack-free times (τ_2) are considerably longer for thicker coatings (76 μm) due to formation of polymeric skin on the top surface decelerating the oxygen diffusion to down surface. As expected, the effect is much stronger at higher metal concentration as the skin formation is faster. Similar effects

are responsible for differences in values of the dry-hard times (τ_3). Very fast skin formation on 76 μm-coatings with high metal concentration is responsible for longer τ_3 than in case of coatings with lower metal content. Such *inverse concentration dependence* is not observed at 38 μm-layers because oxygen becomes available. The formation of thick skin was observed on 76 μm-coatings with cobalt concentration 0.06 and 0.03 wt.%. During the second phase of drying, needle of the drying time recorder has teared off a skin layer that has been forming (not giving a bold uninterrupted path as usual). Development of relative hardness, in the coatings cured with **Co**, seems to be satisfactory for common applications. The values obtained after ten days of curing ($H_{rel;10d}$) exceed 10 % of glass standard and final hardness ($H_{rel;100d}$) vary between 19.1 and 26.9 % depending on the metal concentration (Table 1). The cured coatings of 90 μm-wet thickness are flat and clear without visual defects. Only at metal concentration 0.01 wt.%, thicker edges were observed as a consequence of flow. The test coatings of higher wet thickness (150 μm) show much stronger paint defects. At metal content 0.03 and 0.06 wt.%, liquid binder bellow the polymeric skin caused an effect of orange peel. At 0.01 wt.%, a tendency to flow occurs as a result of slower curing of the polymeric skin.

Driers based on manganese (**Mn**) and vanadium (**V**) show lower activity than **Co** as evidenced by drying time measurements. Manganese(II) 2-ethylhexanoate (**Mn**) gives satisfactory drying times only for 38 μm-coatings. For thicker coatings, dry-hard time (τ_3) exceeds 24 h that is probably caused by skin formation and pure through drying. The coatings, cured with **Mn**, show considerably longer set-to-touch time (τ_1) than in case of **Co** suggesting slower initiation of the autoxidation process (Table 1). Propagation step of the drying process seem to be sufficiently fast as evident from small gaps between τ_1, τ_2 and τ_3 obtained for 38 μm-coatings (*cf.* the gaps with value of τ_1). The main drawback of **Mn** is low final hardness of cured alkyd coatings ($H_{rel;100d} < 13$ %) and high tendency to form visual defects. The films of 90 μm-wet thickness show tiny brush marks. In case of 150 μm-layers, the films flow to edges (0.03, 0.06 wt.% of Mn) or show deeper brush marks (0.01 wt.% of Mn).

Vanadium-based drier (**V**) show satisfactory drying performance only at metal concentration 0.06 wt.% as the dry-hard time does not exceeds 24 h. At this concentration, drying times τ_1, τ_2 and τ_3 on 38-μm layer are comparable with **Co** but behavior of vanadium-based drier seems to be very different. In 76-μm layer, it gives much shorter drying times compared to **Co** (Table 1). It implies more homogenous curing without formation of the skin on top surface. The main advantage of vanadium-based drier is a fast rise of the relative hardness during the cure process. After ten days of curing, the hardness ($H_{rel;10d}$) is comparable to coatings treated with **Co** and final hardness, measured hundred days after application ($H_{rel;100d}$), is even higher than observed for **Co**. Interestingly, high values of final relative hardness were observed also for coatings with low metal content (0.01

and 0.03 wt.%). We note that optimal concentration of **V** (0.06 wt.%) colorizes the 90-µm layers into the light yellow-green. Nevertheless, the coating does not show any other visual defects. Tiny brush marks were observed only in case of 150-µm layer.

Iron bispidine complex (**Fe**) is active at very low metal concentrations (0.0005–0.0030 wt.%). Short drying times were obtained for both 38-µm and 76-µm layers. Skin formation was observed only at metal concentration 0.0030 wt.% (76-µm layer) but even here the dry-hard times is very short (τ_3 = 5.8 h). We note that the drying times τ_2 and τ_3 are dependent on film thickness but the effect is considerably smaller than in case of **Co** and **Mn** implying more homogenous cross-linking comparable to **V**. The main drawback of **Fe** is a very low final hardness of the cured films ($H_{rel;100d}$), which does not reach 10 % of glass standard. The coatings cured with **Fe** have tendency to opacity due to partial miscibility of alkyd formulation with 1,2-propylene glycol, which is used as a solvent in the commercial sample. Such surface defect was observed for 90-µm layer at metal concentrations 0.0030 wt.%; in case of 150-µm layers at 0.0015 wt.% and 0.0030 wt.%.

Table 1. Drying times (τ) [a] relative hardness (H_{rel}) [b] obtained for alkyd formulations of different thickness.

Film thickness	38 µm			76 µm			90 µm	
Drier / conc. (wt.%)	τ_1 (h)	τ_2 (h)	τ_3 (h)	τ_1 (h)	τ_2 (h)	τ_3 (h)	$H_{rel,10d}$ (%)	$H_{rel,100d}$ (%)
Co / 0.06	1.0	1.9	2.6	1.0	6.6 [c]	> 24	14.4	26.9
Co / 0.03	1.5	3.0	3.6	1.7	5.4 [c]	12.9	12.7	23.3
Co / 0.01	3.8	6.6	6.8	4.1	8.0	9.6	10.6	19.1
Mn / 0.06	5.3	7.3	10.8	5.5	12.6 [c]	> 24	7.3	12.9
Mn / 0.03	6.1	8.4	11.1	6.4	11.4 [c]	> 24	6.0	12.8
Mn / 0.01	8.3	10.4	12.9	8.7	12.7	> 24	6.7	12.9
V / 0.06	1.2	3.0	3.8	1.4	3.9	8.0	12.5	31.5
V / 0.03	3.4	11.7	> 24	3.9	9.4	> 24	6.5	27.1
V / 0.01	10.4	> 24	> 24	10.1	> 24	> 24	4.2	22.2
Fe / 0.0030	1.0	2.2	2.6	1.1	3.9 [c]	5.8	5.5	9.6
Fe / 0.0015	1.2	2.2	2.8	1.2	3.5	5.8	5.4	8.7
Fe / 0.0005	2.7	6.7	8.8	2.8	6.2	7.2	5.3	7.6

[a] τ_1 is set-to-touch time; τ_2 is tack-free time; τ_3 is dry-hard time. [b] $H_{rel,10d}$ is relative hardness after 10 days; $H_{rel,100d}$ is final relative hardness reached after 100 days. [c] In time period τ_1–τ_2, the needle tears off a skin from the coating instead of giving a bold uninterrupted path.

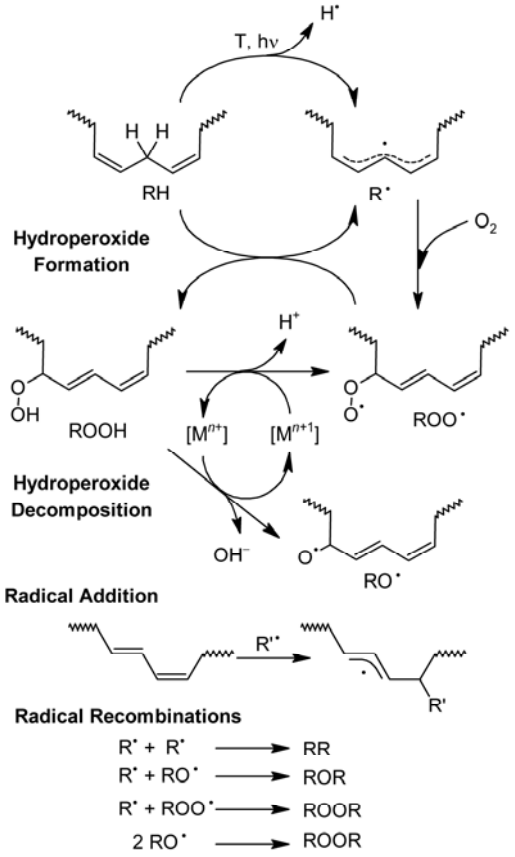

Scheme 2. Simplified mechanism of autoxidation process.

3.2 In situ FTIR spectroscopy

Chemical drying of HS alkyd resin was followed by a time-resolved infrared spectroscopy. The measurements revealed developments typical for autoxidation of unsaturated fatty acids [28]. Briefly, disappearance of antisymmetric *cis*-C=*C–H* stretching band [ν_a(*cis*-C=*C–H*)], observed at 3008 cm^{-1}, follows consumption of isolated *cis* double bonds on the fatty acid tails (Scheme 2). Development of this vibration mode is commonly used for kinetic studies of autoxidation process those were performed on the liquid models of the air-drying paints (*e.g.* fatty acid esters) [15, 26]. As shown in Scheme 2, the autoxidation process gives, in the first step, hydroperoxides with *cis-trans* conjugated double bonds (ROOH). Such kinetically stable intermediates are evidenced by appearance of broad OH stretching band [ν(*O–H*)] at 3400 cm^{-1} and C=*C–H* wagging of *cis-trans* conjugated diene moiety [γ(*cis-trans*-C=C–H)] at 989 cm^{-1}. We note that the changes of the OH stretching band cannot be determined quantitatively as it overlaps with broad bands of water [ν(OH): 3520 and 3300 cm^{-1}], which appears as a side product of hydroperoxide decomposition [20]. Previous studies have further reported a development of isolated *trans*-C=*C–H* wagging at 973 cm^{-1} appearing upon radical addition (Scheme 2) [37].

However, in case of our samples, several vibration modes overlap in this spectral region, which make quantitative determination of isolated *trans*-C=C bonds difficult to perform.

In our previous studies, we have extended aforementioned approach to solvent-borne alkyd resins and estimated kinetic parameters for formulations containing various metal-based driers [10, 11, 19, 20]. The measurements were performed in transmission mode and averaged kinetic data were obtained from overall film profile. We note that this approach is suitable only for formulations, where curing is homogenous at optimal drier concentration at given film thickness. Unfortunately, it is incompatible with HS formulations, used here, owing to very strong thickness effect that may led to incorrect interpretation.

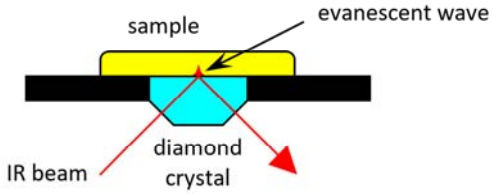

Figure 1. Experimental set-up of ATR-IR study. The infrared radiation is absorbed due to evanescent wave, which penetrates the sample.

3.3 Oxidative drying on the interface air/HS alkyd

Our aim to follow oxidative drying of HS alkyd formulation with strong thickness effect led us to utilize attenuated total reflectance (ATR) sampling technique in conjunction with infrared spectroscopy (Figure 1). This method enables to reach infrared spectra from a thin layer of the coating on the interface sample/ATR crystal (down surface), in which the evanescent wave penetrates. In our experimental setup, depth of penetration varies around 0.67 μm (at 3000 cm^{-1}) depending on refractive index of the sample [38]. The coatings of 30 μm-wet thickness were considered enough thin to be dried homogenously as a bulk with negligible effect of oxygen diffusion. It enables to utilize these measurements as an approach to oxidative drying on the top surface. We note that saturation of the coating with air-oxygen is a necessary condition for determination of kinetic parameters as the autoxidation process is treated as a reaction of pseudo-first order, when the oxygen concentration remains effectively constant [20].

Figure 2 shows development of the *cis*-C=*C–H* stretching and *cis-trans*-C=*C–H* wagging bands for 30 μm-layers of formulations with different concentration of **Co**, **Mn**, **V** and **Fe**. The only exception involves formulations treated with **V**, where the *cis-trans*-C=*C–H* wagging vibration mode could not be followed due to overlap with a strong band of the drier. In this case, Figure 2 reports developments of OH stretching bands instead. We note that OH stretching development for other formulations is given in Supporting Information.

Decrease of ν_a(*cis*-C=*C–H*) in intensity clearly shows that all driers, under study, are active in used concentration ranges. In the 30 μm-layers, the autoxidation is faster at higher metal concentration as evident from shorter half-life of the autoxidation reaction (see $t_{1/2,\ 30\mu m}$ in Table 2). In case of **Co** and **Mn**, the process is very fast in whole concentration range (0.01–0.06 wt.%). Half of the active *cis* double bonds is consumed within few hours (see $t_{1/2,\ 30\mu m}$ in Table 2). The driers based on vanadium and iron are highly active in narrower ranges; 0.03–0.06 and 0.0015–0.0030 wt.%, respectively. At lower metal concentrations, the half-life of the autoxidation reaction exceeds 10 h.

According to previous studies, performed on solvent-borne formulations, the hydroperoxide formation (Scheme 2) could be treated as a reaction of pseudo-first order. Such approximation is applicable on liquid systems saturated with air-oxygen. 30 μm-layers of HS resin **TI870** meet these conditions up to about 50 % conversion as evident from linear parts of logarithmic plots of ν_a(*cis*-C=*C–H*); see Supporting Information.

At metal concentration 0.06 wt.%, cobalt-based drier (**Co**) exhibits very high rate coefficient ($-k_{CH,max}$ = 1.05 h^{-1}) and negligible induction time (IT = 0.1 h) that well correlates with short drying times obtained from mechanical tests on 38-μm layer (*cf.* with data in Table 1). Rapid chemical drying is also visible on fast rise of the C=*C–H* wagging band at 989 cm^{-1} assigned to *cis-trans* conjugated diene moiety (Figure 2). Intensity of the band reaches maximum within 0.8 h and then decreases rapidly due to addition of appeared radicals on conjugated double bond system. We note that such reaction plays important role in autoxidation of air-drying paints, as it is one of the pathways giving crosslinks on the fatty acid tails (Scheme 2). Lowering of the metal concentration led to lower rate coefficient and longer induction time. Nevertheless, even at concentration 0.01 wt.%, the autoxidation process in the 30 μm-layer is fast ($-k_{CH,max}$ = 0.44 h^{-1}).

The formulations, treated with **Mn**, show considerably lower rate coefficient and longer induction time than **Co** at the same metal concentration, which is in line with longer drying times of 38 μm-alkyd layers (Table 1). In case of **V**, sufficient values of $-k_{CH,max}$ were observed in range of concentrations 0.06–0.03 wt.%. At lower metal content, the oxidative drying is very slow ($-k_{CH,max}$ = 0.11 h^{-1}) that results in deterioration of drying activity. The drier based on iron bispidine complex (**Fe**) gives high rate coefficients at very low metal concentrations (0.0015–0.0030 wt.%). Interestingly, the drier exhibits very different development of *cis-trans*-C=*C–H* wagging band than observed for **Co** and **Mn** (Figure 2). After initial fast rise, the band intensity decreases very slowly suggesting limited crosslinking through radical addition mechanism (Scheme 2). Interestingly, this behavior does not have negative effect on drying times probably due to extensive recombination of radicals present in the system.

We note that developments of OH stretching band gives only few more information about the autoxidation process. Shape of its integral plot is very similar to *cis*-C=*C–H* stretching band (for **V** see Figure 2, for other driers see Supporting Information) because the integrated area does not reflect only formation of hydroperoxides but also water, which is their decomposition product.

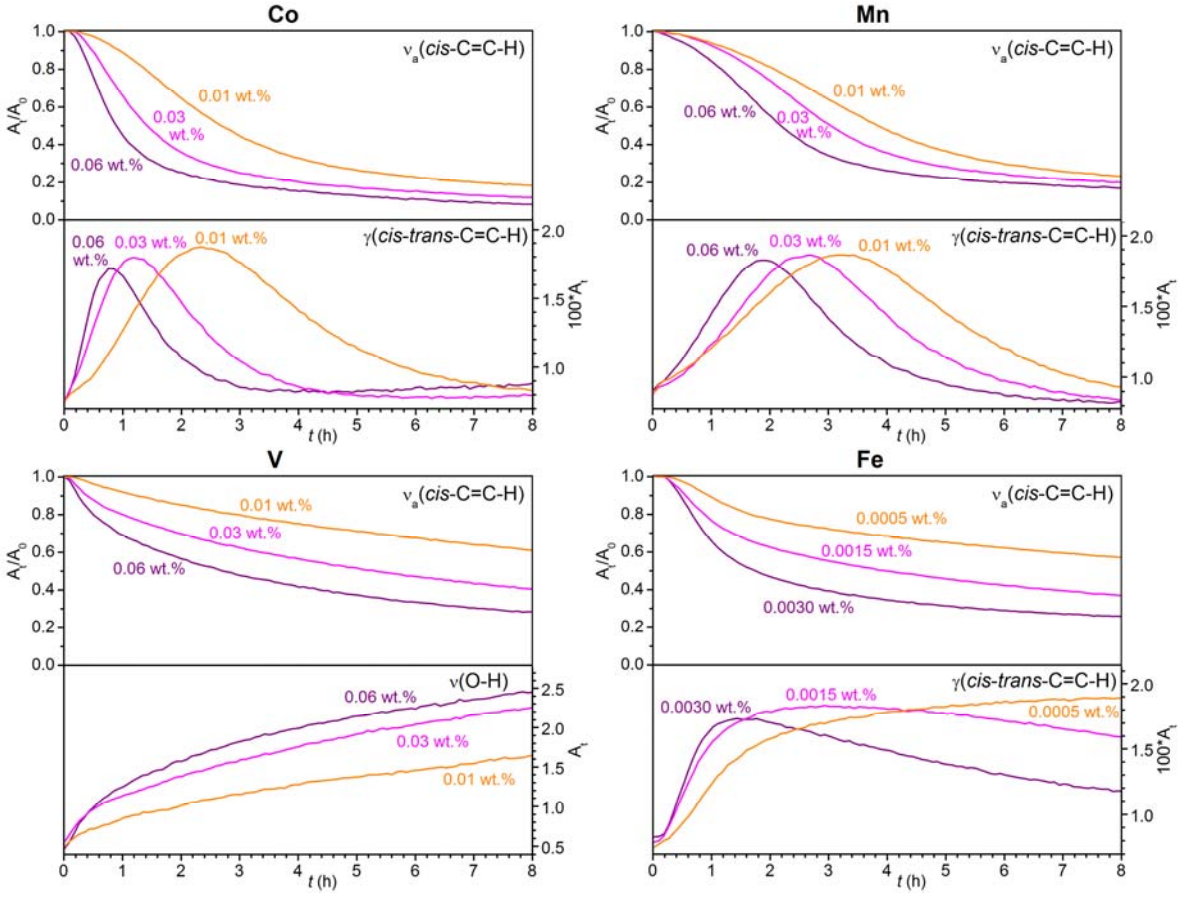

Figure 2. Effect of metal concentration on development of selected vibration modes in alkyd coating of 30 μm-wet thickness.

Table 2. Kinetic parameters ($-k_{CH,max}$, t_{max}, IT, $t_{conj.}$) [a] for the coating saturated with air-oxygen (30 µm-wet thickness) and half-lifes of the process ($t_{1/2}$) for coatings of different film thickness.[b]

Drier / conc. (wt.%)	$-k_{CH,max}$ (h^{-1})	t_{max} (h)	IT (h)	$t_{conj.}$ (h)	$t_{1/2,\ 30\mu m}$ (h)	$t_{1/2,\ 80\mu m}$ (h)	$t_{1/2,\ 130\mu m}$ (h)	$t_{1/2,\ 180\mu m}$ (h)
Co / 0.06	1.05	0.7	0.1	0.8	0.9	1.0	> 20	> 20
Co / 0.03	0.70	1.1	0.2	1.2	1.4	1.4	> 20	> 20
Co / 0.01	0.44	2.8	0.5	2.4	2.7	2.7	11.7	12.2
Mn / 0.06	0.57	2.1	0.9	1.9	2.2	10.2	> 20	> 20
Mn / 0.03	0.43	2.9	1.4	2.7	3.0	6.0	> 20	> 20
Mn / 0.01	0.34	3.6	1.4	3.2	3.9	10.0	> 20	> 20
V / 0.06	0.59	0.2	0.1	– [c]	2.7	2.7	3.1	> 20
V / 0.03	0.38	0.2	0.1	– [c]	5.3	5.1	5.2	> 20
V / 0.01	0.11	0.4	0.2	– [c]	12.6	12.3	11.8	11.4
Fe / 0.0030	0.62	0.7	0.3	1.4	1.8	3.2	7.8	> 20
Fe / 0.0015	0.40	0.7	0.3	3.2	4.0	4.4	5.8	> 20
Fe / 0.0005	0.22	1.0	0.4	8.3	11.2	10.6	10.3	19.4

[a] $-k_{CH,max}$ is maximum autoxidation rate constant observed at time t_{max}; IT is induction time of the autoxidation; t_{conj} is time, in which the band at 989 cm^{-1} reached a maximal absorbance. [b] $t_{1/2}$ is half-life of the autoxidation. It was estimated for various film thickness on the down surface of the coating. [c] not estimated.

3.4 Effect of film thickness on autoxidation process

Although ATR technique cannot be used for direct profiling of the coating as aforementioned confocal Raman microscopy or spatial resolved NMR techniques [16, 30-32], the monitoring of a thin layer at the interface coating/ATR crystal enables to follow thickness effects on series of samples with the same composition but different film thickness (Figure 3). In our case, series of four independent experiments were used for each formulation under study. The wet thickness of the samples was set by frame applicator of given gap (30, 80, 130 and 180 µm). The obtained data were used as an approach to drying profile of paint film of 180 µm-wet thickness.

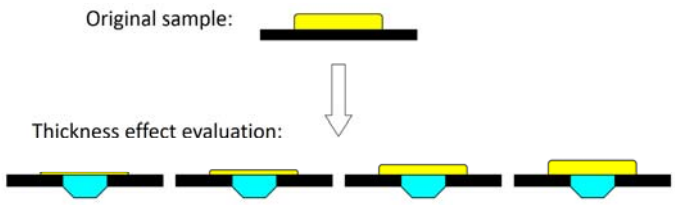

Figure 3. Evaluation of thickness effect on a sample of alkyd formulation. The series of ATR-IR experiments with different film thickness are performed to approach profiling of a thick coating.

The comparison of time-resolved infrared spectra obtained for samples of different thickness proves that formulations of **Co** are cured homogenously up to 80 µm-wet thickness in whole concentration range. It is evident mainly from developments of ν_a(*cis*-C=*C–H*) shown in Figure 4 (*cf.* 30 µm and 80 µm for **Co** in Figure 4). The same behavior of 30 µm and 80 µm-layer was also noticeable on developments of γ(*cis-trans*-C=C–H) and ν(O–H); see Supporting Information. In coatings thicker than 80 µm, large part of reactive double bonds stays intact at the interface coating/ATR-crystal; see parameters $t_{1/2}$ in Table 2. Such observation implies formation of densely crosslinked skin in the top surface that blocks oxygen diffusion into substrate side of the coating. As expected, rate of *permanent skin formation* is given by concentration of the drier. At 0.06 wt.%, it appears very fast and almost no oxygen is diffused to substrate side of the coating as evident from development of *cis*-C=*C–H* stretch (Figure 4). The observed consumption of the isolated *cis*-double bonds is only due to reaction with oxygen dissolved during preparation of the formulation. Low concentration of radicals in the substrate side of the coating is further evidenced by development of γ(*cis-trans*-C=C–H); see Figure 5. After initial rise, the concentration of *cis-trans* conjugated double bonds stays constant implying negligible crosslinking via radical addition pathway (Scheme 2).

At lower metal concentration, the reaction rate decreases, which allows oxygen to diffuse even through 180 µm-film. Consequently, at the bottom of the sample, one sees a faster curing because oxygen becomes available. Higher conversion of the isolated *cis*-double bonds is revealed from the development of *cis*-C=*C–H* stretch shown in Figure 5. At 0.01 wt.%, the concentration of radicals at bottom of 180 µm-samples is enough high to initiate crosslinking via radical addition mechanism. It is evident from development of the γ(*cis-trans*-C=C–H) as a slow decrease on the curve (Figure 5).

Formulations, treated with **Mn**, form very thin polymeric skin at the beginning of the drying process as evident from developments of the infrared spectra at the interface sample/ATR crystal. Up to ~30% conversion, the coatings of 30 and 80 µm-wet thickness show very similar development of the *cis*-C=*C–H* stretching band (Figure 4). After this period, autoxidation of latter coating is decelerated due to limited oxygen penetration

through the appeared thin skin. Interestingly, autoxidation process reaccelerates after some time as the skin becomes thicker. Such behavior is known as *front-forming drying* and was previously described in detail by spatial resolved NMR techniques [22]. We note that autoxidation of 130 and 180 µm-coating is very slow. In both cases, air-oxygen cannot penetrate to the bottom of the coating due to densely crosslinked skin similarly as in case of coatings treated with **Co**. Lowering **Mn** concentration has only minor effect on through-drying of the thick coatings (Figure 5). Indeed, the half-life of the autoxidation exceeds 20 h even at 0.01 wt.%; see $t_{1/2}$ in Table 2.

Vanadium-based drier (**V**) cures the HS alkyd binder more homogenously than other driers under study. At metal concentrations 0.03 and 0.06 wt.%, spatially *homogenous drying* was observed for coatings up to wet thickness 130 µm as revealed from the developments of *cis*-C=*C–H* stretching and O–H stretching bands (*cf.* 30 µm, 80 µm and 130 µm for **V** in Figure 4 and in Supporting Information). At metal concentration 0.01 wt.%, oxidative drying of the formulation is very slow but homogenous up to 180 µm-wet thickness.

Excellent through drying was observed on formulations treated with **Fe**. Although aforementioned mechanic test revealed formation of polymeric skin at metal concentration 0.0030 wt.%, the air-oxygen can diffuse at the bottom of the 130 µm-coatings as evident from developments of ν_a(*cis*-C=*C–H*). It is due to sparse crosslinking that keeps the polymer permeable. Comparison of the 30, 80 and 130 µm-coatings reveals strong spatial inhomogeneity of the cure process suggesting that oxygen penetration through the skin is slower that consumption in the coating. As a result, the coating is not saturated with air-oxygen and substrate side of the coatings are cured slower. The formation of thin skin could be avoided by lowering of the metal concentration. At 0.0015 wt.%, the cure process is fully homogenous up to ~130 µm-wet thickness. Deceleration of autoxidation at the down surface of coating was observed only for 180 µm-coating, where half-live of autoxidation exceeds 20 h. Even more uniform through drying can be ensured by further lowering of metal concentration to 0.0005 wt.% as evident from more uniform development of ν_a(*cis*-C=*C–H*) at different wet thickness (Figure 4). We note that conversion of reactive isolated *cis* double bonds at the interface coating/ATR crystal rises with lowering of metal concentration in 180 µm coatings (Figure 5), which could be taken as a prove of better through drying at lower drier dosage.

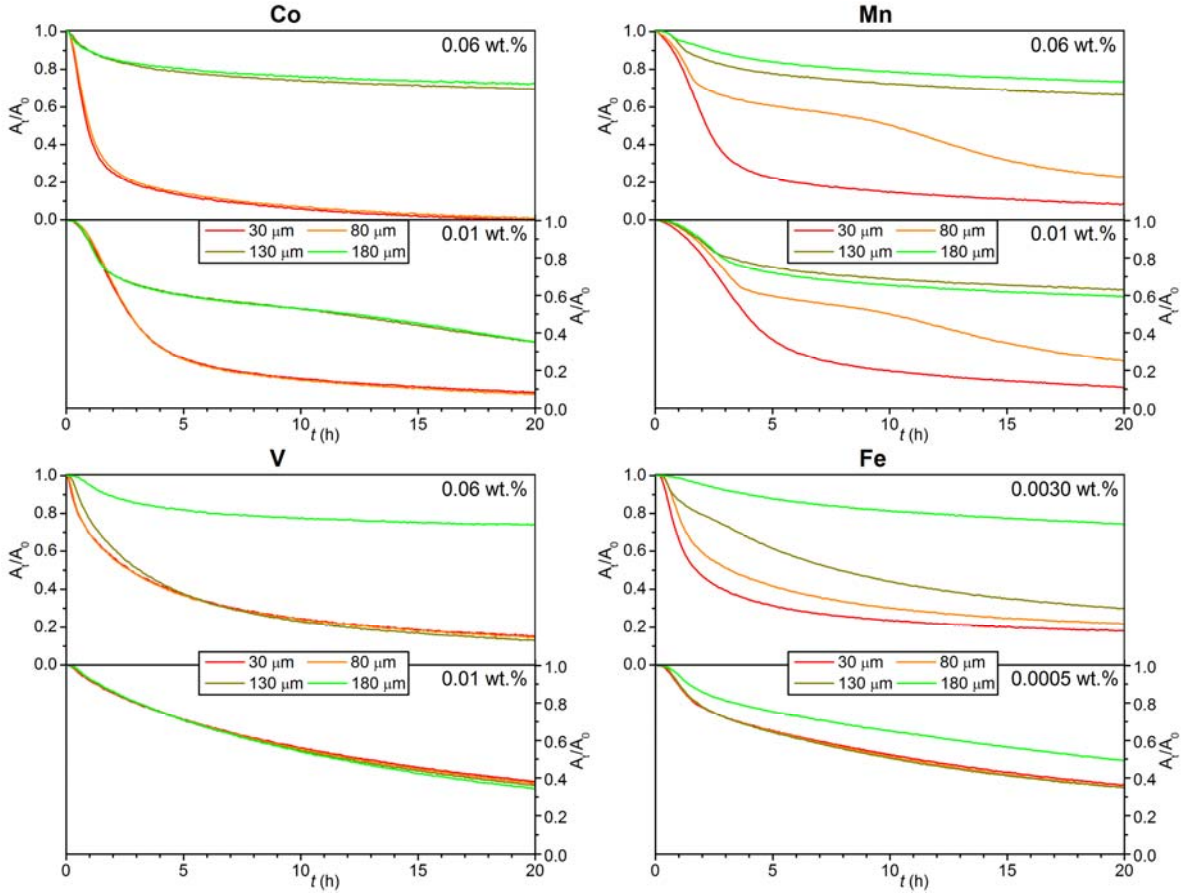

Figure 4. Effect of wet thickness on development of *cis*-C=*C*–*H* stretching in alkyd formulations treated with different driers.

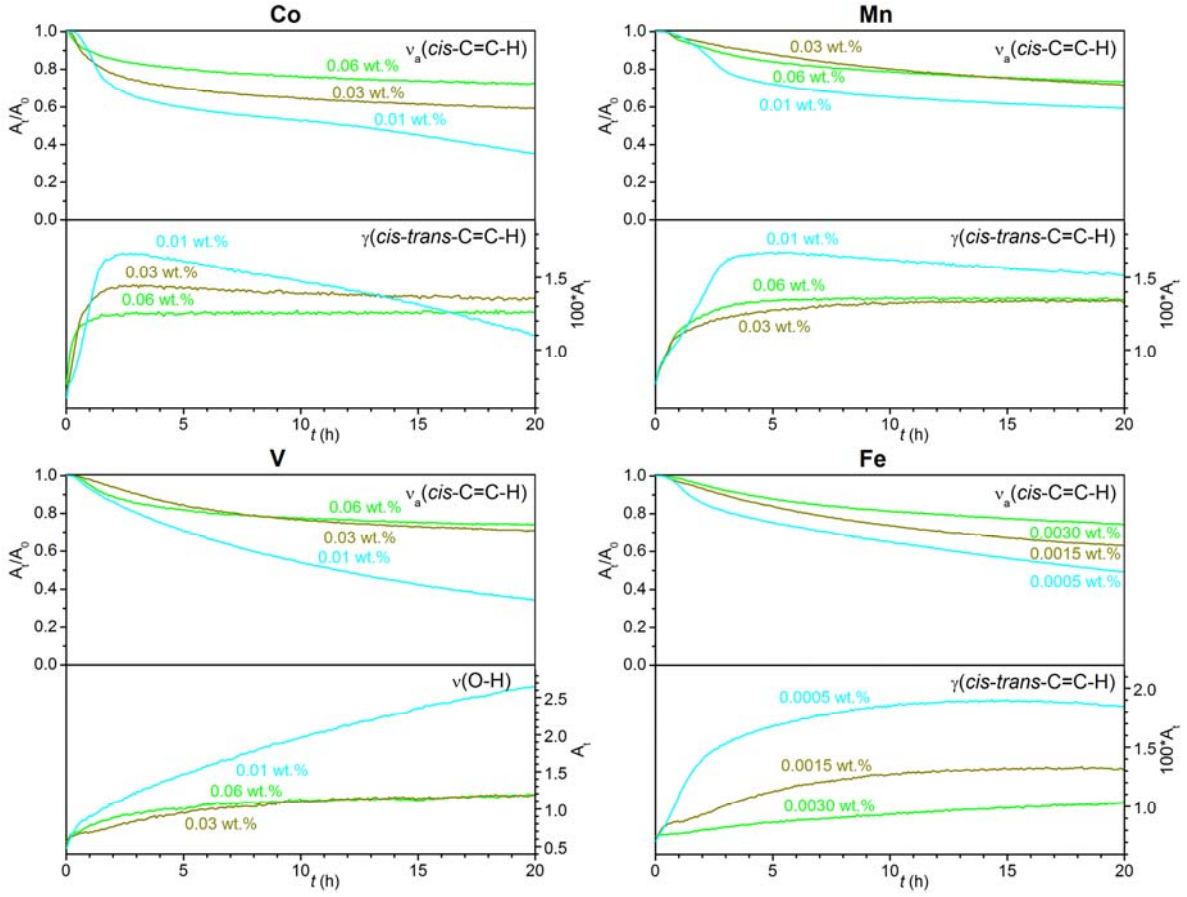

Figure 5. Effect of metal concentration on development of selected vibration modes in alkyd coating of 180 µm-wet thickness.

4. Conclusion

Our in-depth ATR-IR study, supported with classical mechanical studies, enabled to compare four commercially available primary driers and to resolve two well-distinguished modes of film-formation (*i.e.* front front-forming and homogenous drying) in our systems drier/binder. For detailed comparison, profiling of 130 µm-paint coatings was approached by three independent ATR-IR experiments of different wet paint thickness. The experiments on 30 µm-layers approached the top surface saturated with air-oxygen while those on 80 µm- and 130 µm-layers the inner space and the down surface of the coatings, respectively.

This model reveals that each drier under study shows very specific curing properties. The cobalt-based drier (**Co**) is very powerful in studied concentration range as documented by high rate coefficient ($-k_{CH,max}$). It forms a densely crosslinked skin on the coating, which is not permeable for air-oxygen. Due to the *permanent skin formation* (see Figure 6), film-formation process is practically ceased and down surface of the 130 µm-coatings stays unreacted at least for six months, which was verified by infrared spectroscopy. We note that the specific

behavior of **Co** is probably not caused by a higher concentration of the drier on the interface air/alkyd (surfactant-like effect) because skin removal restarts the autoxidation process with kinetic behavior very similar to freshly prepared 30 µm-layer.

The manganese-based drier (**Mn**) was found to be less powerful than **Co** at given concentrations as evident from lower $-k_{CH,max}$ but even here the skin formation is well documented by ATR-IR experiments. The appearing skin seems to be much thinner and less densely crosslinked than in case of **Co**. It allows oxygen to diffuse slowly into the film while the skin becomes thicker. In case of **Mn**, the *front-forming drying* (Figure 6) is very slow. The 130 µm-coatings are not through dried within 24 hours as documented by both ATR-IR and standard mechanical tests.

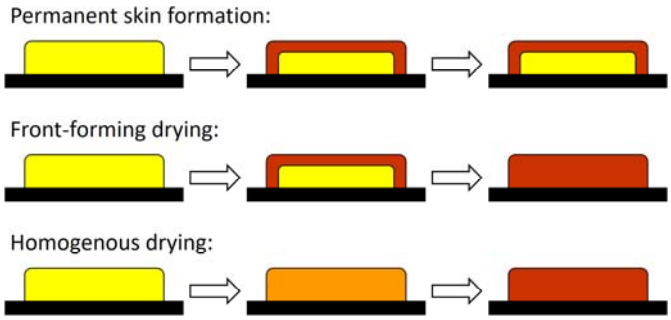

Figure 6. Schematic view of film-formation process.

A good example of fast *front-forming drying* was observed at high concentrations of the iron-based drier (**Fe**). The mechanical tests confirmed a formation of polymeric skin but much less densely crosslinked than observed for **Mn**. At metal concentration 0.0030 wt.%, ATR-IR experiments revealed very different developments in each model coating implying high gradient of oxygen concentration in the 130 µm-layer. It may only occur when air-oxygen consumption is fast but the polymeric skin stays well permeable. We note that autoxidation is, in this case, very fast. According to infrared data, the 130 µm-coating is through dried within 24 hours.

Lowering of **Fe** concentration to 0.0005 wt.% decelerates the autoxidation process and *homogenous drying* (Figure 6) of whole 130 µm-coating was revealed from very similar developments in the model coatings. The drying process become homogenous because the consumption of oxygen is slower that its diffusion from air. The *homogenous drying* was also observed in all formulations of vanadium-based drier (**V**). At metal concentrations 0.01 wt.%, rate of autoxidation is as slow that even 180 µm-coating is dried homogenously.

In summary, this study has proven that ATR-IR technique is very suitable for investigation of thickness effect on samples of air-drying binders. Although it does not enable a direct sample profiling as confocal Raman microscopy and NMR imaging, the model made from several independent measurements gives a comprehensive

view of through drying of the coatings. The main advantage of here presented approach is a wide availability of ATR-IR technique. It is commonly used not only in academic environment but also in the chemical industry for "quality control" or "research and development". We note that single ATR-IR experiment enables to determine kinetic parameters of the autoxidation process. For this purpose, it is necessary to prepare a film thin enough to avoid effects of oxygen transport, which enables to focus on investigating the chemistry only.

Acknowledgements

This work was supported by Ministry of Education of the Czech Republic (Project No. UPA SG370006).

References

[1] F. N. Jones, in *Ullmann's Encyclopedia of Industrial Chemistry*, **2003**, pp. 429-446.

[2] A. Hofland, Prog. Org. Coat. 73 (2012) 274-282.

[3] D. Nelson, in *Paint and Coating Testing Manual: 15th Edition of the Gardner-Sward Handbook* (Ed.: J. V. Koleske), ASTM International, West Conshohocken, **2012**, pp. 65-71.

[4] J. Lindeboom, Prog. Org. Coat. 34 (1998) 147-151.

[5] M. Manea, *High Solid Binders*, Vincentz, Hannover, **2008**.

[6] R. van Gorkum, E. Bouwman, Coord. Chem. Rev. 249 (2005) 1709-1728.

[7] M. D. Soucek, T. Khattab, J. Wu, Prog. Org. Coat. 73 (2012) 435-454.

[8] D. Lison, M. De Boeck, V. Verougstraete, M. Kirsch-Volders, Occup. Environ. Med. 58 (2001) 619-625.

[9] M. De Boeck, M. Kirsch-Volders, D. Lison, Mutat. Res. 533 (2003) 135-152.

[10] O. Preininger, J. Vinklárek, J. Honzíček, T. Mikysek, M. Erben, Prog. Org. Coat. 88 (2015) 191-198.

[11] O. Preininger, J. Honzíček, P. Kalenda, J. Vinklárek, J. Coat. Technol. Res. 13 (2016) 479-487.

[12] O. Preininger, I. Charamzová, J. Vinklárek, I. Císařová, J. Honzíček, Inorg. Chim. Acta 462 (2017) 16-22.

[13] I. Charamzová, J. Vinklárek, P. Kalenda, J. Honzíček, Coatings 8 (2018) 204.

[14] E. Bouwman, R. van Gorkum, J. Coat. Technol. Res. 4 (2007) 491-503.

[15] S. T. Warzeska, M. Zonneveld, R. van Gorkum, W. J. Muizebelt, E. Bouwman, J. Reedijk, Prog. Org. Coat. 44 (2002) 243-248.

[16] Z. O. Oyman, W. Ming, R. van der Linde, J. ter Borg, A. Schut, J. H. Bieleman, Surf. Coat. Int. B Coat. Trans. 88 (2005) 269-275.

[17] J. W. de Boer, P. V. Wesenhagen, E. C. M. Wenker, K. Maaijen, F. Gol, H. Gibbs, R. Hage, Eur. J. Inorg. Chem. (2013) 3581-3591.

[18] B. Pirš, B. Znoj, S. Skale, J. Zabret, J. Godnjavec, P. Venturini, J. Coat. Technol. Res. 12 (2015) 965-974.

[19] M. Erben, D. Veselý, J. Vinklárek, J. Honzíček, J. Mol. Catal. A: Chem. 353-354 (2012) 13-21.

[20] M. Křižan, J. Vinklárek, M. Erben, I. Císařová, J. Honzíček, Prog. Org. Coat. 111 (2017) 361-370.

[21] J. Honzíček, J. Vinklárek, J. Appl. Polym. Sci. 135 (2018) 46184.

[22] Ö. Gezici-Koç, C. A. A. M. Thomas, M. E. B. Michel, S. J. F. Erich, H. P. Huinink, J. Flapper, F. L. Duivenvoorde, L. G. J. van der Ven, O. C. G. Adan, Mater. Today Commun. 7 (2016) 22-31.

[23] S. J. F. Erich, Ö. Gezici-Koç, M. E. B. Michel, C. A. A. M. Thomas, L. G. J. van der Ven, H. P. Huinink, J. Flapper, F. L. Duivenvoorde, O. C. G. Adan, Polymer 121 (2017) 262-273.

[24] L. Dubrulle, R. Lebeuf, M. Fressancourt-Collinet, V. Nardello-Rataj, Prog. Org. Coat. 112 (2017) 288-294.

[25] W. J. Muizebelt, M. W. F. Nielen, J. Mass Spectrom. 31 (1996) 545-554.

[26] L. Dubrulle, R. Lebeuf, L. Thomas, M. Fressancourt-Collinet, V. Nardello-Rataj, Prog. Org. Coat. 104 (2017) 141-151.

[27] L. F. Sturdy, A. Yee, F. Casadio, K. R. Shull, Polymer 103 (2016) 387-396.

[28] F. R. van de Voort, A. A. Ismail, J. Sedman, G. Emo, J. Am. Oil Chem. Soc. 71 (1994) 243-253.

[29] G. Ellis, M. Claybourn, S. E. Richards, Spectrochim. Acta 46A (1990) 227-241.

[30] B. Marton, L. G. J. van der Ven, C. Otto, N. Uzunbajakava, J. V. Vancso, Polymer 46 (2005) 11330-11339.

[31] S. J. F. Erich, L. G. J. van der Ven, H. P. Huinink, L. Pel, K. Kopinga, J. Phys. Chem. B 110 (2006) 8166-8170.

[32] S. J. F. Erich, J. Laven, L. Pel, H. P. Huinink, K. Kopinga, Prog. Org. Coat. 55 (2006) 105-111.

[33] *ASTM D5895-03, Standard Test Methods for Evaluating Drying or Curing During Film Formation of Organic Coatings Using Mechanical Recorders*, ASTM International, West Conshohocken, PA, **2003**.

[34] *ISO 1522:2006, Paints and varnishes - Pendulum damping test*, International Organization for Standardization, **2006**.

[35] B. Persoz, Peintures, Pigments, Vernis 21 (1945) 194-201.

[36] *ISO 2409:2013, Paints and varnishes - Cross-cut test*, International Organization for Standardization, **2013**.

[37] Z. O. Oyman, W. Ming, R. van der Linde, Prog. Org. Coat. 48 (2003) 80-91.

[38] B. C. Smith, in *Fundamentals of Fourier Transform Infrared Spectroscopy, Second Edition*, CRC Press, **2011**, pp. 129-146.